Impact of the Lorentz Force on Electron Track Structure and Early DNA Damage Yields in Magnetic Resonance-Guided Radiotherapy

Yoshie Yachi
Hokkaido University
Takeshi Kai
Japan Atomic Energy Agency (JAEA)
Yusuke Matsuya
Japan Atomic Energy Agency (JAEA)
Yuho Hirata
Japan Atomic Energy Agency (JAEA)
Yuji Yoshii
Hokkaido University
Hiroyuki Date (date@hs.hokudai.ac.jp)
Hokkaido University

Research Article

Keywords:

Posted Date: January 14th, 2022

DOI: https://doi.org/10.21203/rs.3.rs-1248701/v1

Abstract

Magnetic resonance-guided radiotherapy (MRgRT) has been developed and installed in recent decades for external radiotherapy in several clinical facilities. The Lorentz force modulates dose distribution by charged particles in MRgRT; however, the impact by this force on low-energy electron track structure and early DNA damage induction remain unclear. In this study, we estimated features of electron track structure and biological effects in a static magnetic field (SMF) using a general-purpose Monte Carlo code, Particle and Heavy Ion Transport code System (PHITS) that enables us to simulate low-energy electrons down to 1 meV by track-structure mode. The macroscopic dose distributions by electrons above approximately 300 keV initial energy in liquid water are changed by both perpendicular and parallel SMFs against the incident direction, indicating that the Lorentz force plays an important role in calculating dose within tumours. Meanwhile, DNA damage estimation based on the spatial patterns of atomic interactions indicates that the initial yield of DNA double-strand breaks (DSBs) is independent of the SMF intensity. The DSB induction is predominantly attributed to the secondary electrons below a few tens of eV, which are not affected by the Lorentz force. Our simulation study suggests that treatment planning for MRgRT can be made with consideration of only changed dose distribution.

Introduction

Magnetic resonance-guided radiotherapy (MRgRT) has been developed to achieve high tumour control probability (TCP) with suppressed side effects by virtue of real-time imaging of soft tissues with high contrast.[1] In recent decades, MRgRT employing photon beams, such as linear accelerated X-rays or ^{60}Co γ-rays, in static magnetic fields (SMF) for MR imaging[1,2] has been installed in several clinics. When treating tumours with the MRgRT system, electron beams as well as secondary electrons generated by photons can be affected by the Lorentz force in transverse SMF against incident beams, leading to dose enhancement, the so called electron return effect (ERE).[3] To date, some biological experiments have shown enhanced radio-sensitivities (e.g., chromosome aberration and cell death) even at the same dose level in magnetic fields,[4–7] whereas others have suggested that radio-sensitivities of X-ray irradiation are unaffected by magnetic fields[8–10]. Because the experimental results in the literature do not show consistent results, the radio-sensitivity under magnetic fields remains uncertain. In order to clarifying the radiosensitivity, it is necessary to evaluate the relationship between radiation track structure and biological impacts.

To investigate the impact of magnetic fields on radiation-induced biological effects based on the radiation track structure, a Monte Carlo computational simulation for radiation transport is a powerful approach. There are several Monte Carlo codes for simulating electron track structure developed worldwide.[11–13] Amongst the codes, PENELOPE[14,15] and Geant4-DNA[16–19] have provided micro- and nano-dosimetric quantities in magnetic fields, making clear the biological impact in SMFs.[20,21] These simulations have suggested no significant enhancement of dose deposition at the DNA scale in SMFs.[20,21] However, to our knowledge there is no report estimating the various types of DNA damage

yields, i.e., double-strand breaks (DSBs) and other complex interactions. Besides, the model to presume DNA damage yields is still under development, so it is of importance to estimate early DNA damage yields utilizing the first-principles method.

For dealing with the above issues, Particle and Heavy Ion Transport code System (PHITS)[22] is appropriate because the dynamics of low-energy electrons down to 10^{-3} eV in liquid water[23–28] can be analysed using the electron track-structure mode, *etsmode*, even in magnetic fields, where the types and the yields of DNA damage are determined based on the spatial patterns of atomic interactions.[29–31] In this study, we estimate the physics features of electron tracks (i.e., ranges, dose distributions, etc.) in SMFs and the early DNA damage yields through physics process simulations. This work finally shows that treatment planning for MRgRT can be made considering both change of dose distribution and unaffected biological impact.

Materials And Methods

Simulation setup for electron transport in SMF

PHITS code version 3.26[22] was used for simulating electron tracks in liquid water. In the PHITS simulations, the [track-structure] section was activated within liquid water, which enables us to calculate each atomic interaction (i.e., elastic scattering, ionization, electron excitation, dissociative electron attachment, vibrational excitation, rotational excitation and phonon excitation) along an electron track based on *etsmode*[31,32]. To consider the Lorentz force in the PHITS simulation, we also used the [magnetic field] section for electrons and positions.

Electron track structure analysis and calculation of physical quantities

Dose distributions by 10-MeV electrons parallel to the SMF along the x- and y-axes, and 1-MeV electrons perpendicular to the SMF along the x- and z-axes were calculated by the electron gamma shower (EGS)[33] mode in PHITS, which is a condensed-history approach for simulating electron kinetics for energies down to 1 keV. The two types of ranges, i.e., penetration length and projected range, were also calculated. It should be noted that the penetration length is defined as the length of the vector from the point of departure to the final position of the electron after thermalization, whereas the projected range is the length between the departure and the final position projected to the axis in the incident direction. These ranges of electrons with monoenergetic energy from 100 to 1000 keV in various SMF intensities were calculated.

To verify the simulation accuracy of *etsmode* in the SMF, we compared the result of PHITS *etsmode* with that of EGS. The cut-off energies for *etsmode* and EGS were 1.0 eV and 1.0 keV, respectively. In addition, we simulated the electron tracks in vacuum for checking the electron trajectory changed by the SMF (without electron scattering by the interaction with liquid water). Since PHITS estimates the radiation

track from the corresponding mean-free path without considering a constant time interval (i.e., 1 attosecond), we adopted a time-dependent variational Monte Carlo method, dynamic Monte Carlo code (DMCC).[23–28] The physical model for simulating electron dynamics by DMCC was implemented in *etsmode*, thus the validation using DMCC can be applied to the calculation results using *etsmode*. From the DMCC simulation, we obtained the gyration time and radius of the electrons in one period within the SMF. Various electron energies (0.01-1000 keV) were also simulated and compared with the projected range 50-1000 keV.

Estimation of DNA damage yields

To evaluate the impact of magnetic fields on DNA damage yields, we used an analytical code for estimating DNA damage implemented in PHITS version 3.26. In the analytical code, the spatial patterns of the inelastic interactions (i.e., ionization and excitation) calculated by *etsmode* were derived.[29] To estimate DSB yield (Y_{DSB}), it is assumed that the frequency of linkage N_{link} (combination of two events generated within 10 bp) per energy deposition E_{in} is proportional to Y_{DSB} as given by

$$Y_{DSB}(E_{in}) = k_{DSB}\frac{N_{link}}{E_{in}} \qquad (1)$$

where k_{DSB} is the proportionality constant (keV/Gy/Da).

Based on this formula, we obtained the Y_{DSB} values for 0.1, 1.0, 10, 100, 300 keV electrons in SMF intensities B from 0.0 to 10.0 (T). To quantitatively evaluate the secondary electron impact, we also deduced the Y_{DSB} value when not considering the generation of secondary and Auger electrons. In addition, we estimated the fraction of clustered forms, known as complex DSBs, based on a previous study.[30] The DSBs were classified into the DSB coupled with a SB within 10 bp (denoted as DSB+) and DSB coupled with two SBs within 10 bp (denoted as DSB++).[34] To identify the DSB complexity, we counted the number of interactions (i.e., ionization and excitation) in a sampling site within a 10 bp radius sphere at a DSB site (weight of linkage) N_{cl}, namely $2 \leq N_{cl} < 14$ for simple DSB, $14 \leq N_{cl} < 26$ for DSB+, and $26 \leq N_{cl} < 38$ for DSB++.

Results And Discussion

Electron dose distribution in magnetic fields

The dose distributions for 10-MeV electrons parallel to SMFs (B = 0.0, 5.0, 10.0 T) are shown in Figs. 1 (A) and (B). The track structure for 10-MeV electrons at 0.0 T is shown in Fig. 1 (C). In the case of the field parallel to the incident electron direction, the larger the SMF strength, the narrower to the x- or y-axis the electron beams is (Fig. 1 (A)). The depth-dependency of dose (y-axis) is independent of the SMF (Fig. 1 (B)). Meanwhile, the dose distributions for 1-MeV electrons perpendicular to SMFs (B = 0.0, 5.0, 10.0 T) are shown in Figs. 1 (D) and (E). The track structure for 1-MeV electrons at 0.0 T is shown in Fig. 1 (F).

The dose distribution without a SMF is symmetrical with respect to x=0. However, those perpendicular to SMFs are largely biased in a large SMF strength (Fig. 1 (D)). Focusing on depth-dependencies perpendicular to the SMF, as the SMF becomes larger, the energies are deposited over less depth (Fig. 1 (E)). The change of dose distributions is analogous to the modification of track structures confirmed in supplementary data (see Fig S1). Note that the distributions calculated by *etsmode* were confirmed in supplementary data (see Fig. S2) and these results were in good agreement with the calculated results by EGS.

The results by PHITS simulation show that the trajectories of 10-MeV and 1-MeV electrons, which are used in radiation therapy, are significantly affected by magnetic fields. However, we confirmed that the dose distributions by low-energy electrons are not affected by the SMF as shown in supplementary data (see Fig. S3).

Impact of magnetic fields on projected ranges of electrons

Figure 2 shows the ranges of electrons perpendicular to the SMF as a function of incident electron energy. To verify the accuracy of electron track structure in the SMF simulated by *etsmode*, we compared the electron ranges calculated by to those by EGS. The simulation accuracy of *estmode* in the absence of a SMF has been extensively discussed in comparison with the recommended values of ICRU reports and experimental data reported previously.[29] As shown in Fig. 2, we compared the range given by *etsmode* to that by EGS, further affirming the accuracy of *etsmode* even in magnetic fields.

The calculated ranges for monoenergetic electrons in the absence of a SMF (B = 0.0 T) are shown in Fig. 2 (A), where the incident energy range was set to be 50-1000 keV because significant SMF effects can be expected. The projected range for monoenergetic electrons (100-1000 keV) as a function of the SMF intensity (B = 0.0-10.0 T) are also shown in Fig. 2 (B); there are no significant SMF effects on projected ranges for 100-keV electrons. Meanwhile, in the case of electrons with high energies above 300 keV in the presence of SMF intensity over 3.0 T, the larger the SMF strength becomes, the shorter the projected range is. These simulation results suggest that the travelling lengths along the z-direction are shortened due to the Lorenz force within the SMF, and the macroscopic dose distributions can be modified by the SMF and projected range in the SMF is shorten compared to that in non-SMF.

Assuming the high-energy electron beams used in radiation therapy, the electrons with incident energy over 1 MeV locally deposit their energies in the region close to the departure point of incident electrons (see Fig. 1 (E)). It was therefore confirmed that the SMF effects (so called electron return effect (ERE)) for electrons in liquid water largely depend on the flight length and time. Also, the simulation shows that the dose distribution within solid tumours and normal tissues should be calculated in consideration of magnetic fields when making treatment planning.

Estimation of electron return effects in vacuum

The gyration time and radius of electrons in vacuum in the presence of a SMF (B = 0.0-10.0 T) was evaluated using DMCC. These calculations assume that the electrons are in vacuum without considering

atomic interactions. Figure 3 (A) shows the relationship among incident electron energies, time and radii. The time is constant up to approximately 100 keV, then exponentially increases above 100 keV. The radius also exponentially increases in the energy range from 0.01 to 1000 keV. In a previous study[20], the gyration radii for electrons (0.001-100 MeV) in vacuum applied by magnetic fields were compared with the continuous slowing down approximation (CSDA) range. This result shows that electrons with energy above 100 keV, in which the CSDA range is longer than the gyration radius, are modified by the SMF (below 10.0 T). In contrast, we show the relationship between the time and the radii of low-energy electrons in vacuum (Fig. 3 (A)). It was confirmed that the flight distance and time until attenuation due to the interaction with water is shorter than the radius and the time in one period in the energy of electrons (below a few hundreds of keV). From this relation, it was found that the electrons below a few hundreds of keV slow down immediately before they drift by SMF (i.e., a few hundreds of psec).

Figure 3 (B) shows the comparisons of projected range and the gyration radii under B=3.0 (T) in liquid water and in vacuum. The projected range under B=0.0 (T) is also depicted in Fig. 3 (B). In the case of high-energy electrons (100-1000 keV), the gyration radius monotonically increases from 0.37 to 1.58 mm as the electron kinetic energy gets higher. The radius becomes closer to the projected range. In the case of low-energy electrons (0.01-90 keV), the radius is significantly larger compared to the projected length. Therefore, high energy electrons drift in the presence of a SMF. From the relations shown in Fig. 3, it was further confirmed that the electrons with higher kinetic energy than 100 keV can be strongly affected by the SMF.

DNA damage yields for monoenergetic electrons in a SMF

The DSB yield, Y_{DSB}, by monoenergetic electrons in the SMFs (B = 0.0-10.0 (T)) are shown in Fig. 4 (A). In the range of incident electron energy from 0.1 to 300 keV, there is no SMF impact on Y_{DSB} for various intensities of magnetic field in both parallel and perpendicular orientations. The DNA damage simulation based on *etsmode* suggests that the SMF effects do not appear at the DNA (nanometer) scale. When irradiating high-energy electrons in liquid water, uncountable secondary electrons with several dozen eV and Auger electrons with about 500 eV from the inner shells are generated. These results suggest that the secondary electrons may be intrinsically related to the induction of DSBs.

To illustrate the contribution of secondary electrons to DSB induction, we also estimated Y_{DSB} without considering the secondary electrons or Auger electrons. The result is shown in Fig. 4 (B). Focusing on 100-keV electrons, the Y_{DSB} value without any secondary electrons including Auger electrons (red circles and lines) becomes lower than that with all secondary electrons (blue circles and lines). Furthermore, the Y_{DSB} value without any secondary electrons is almost zero. The maximum value of Y_{DSB} without any secondary electrons is 1.51 in the case of 0.4-keV electrons, which is about half the value for Y_{DSB} = 3.35 when considering all secondary electrons. These results indicate that the secondary electrons including Auger electrons are major contributors to induce DSBs for high energy electrons (over 100 keV). Low-energy secondary electrons can be produced by inelastic interactions within a few fsec[24,27], and the corresponding penetration length is approximately 10 nm. Also, as shown in Fig. 3, the gyration time and

radius to induce SMF impact on the secondary electrons are more than several ps and several μm, respectively. The secondary electrons therefore slow down before being affected by a magnetic field. In Fig. 3B, the Y_{DSB} values of high-energy electrons (over 100 keV) were lower than that of 100-keV electrons. This is because the cross sections for higher energy part is based on vapour phase. In the vapour phase, the number of ionization events is estimated to be fewer than that in the liquid phase.

Figure 5 (A) shows that the ratio of DNA damage complexity (cDSB/DSB) for 300 keV electrons is larger than that of 100 keV electrons. The cDSB/DSB for both electron energies decreases in the case of no Auger electrons. In addition, the cDSB/DSB of 100 keV and 300 keV electrons for various intensities of the SMF is shown in Fig. 5 (B). cDSB/DSB is independent of the intensity of the SMF. These results are corelated with the fact that Auger electrons contribute to DNA damage complexity and the energy of electrons is not enough to be affected by the SMF (Fig. 3).

The present estimation for DNA damage yields based on physical processes suggests no significant biological impact caused by SMFs. This may be useful for interpreting the experimental data on surviving fractions after X-ray irradiation in the SMF.[8–10] However, some reports suggest the cell-killing effects for low LET radiation increases in the direction parallel to the SMF.[6,7] Y_{DSB} calculated in this study was only based on the physical interaction with electrons and biological tissues after irradiation. It is also necessary to discuss the effect of the SMF on the chemical phase or biological phase. Since the energy range of electrons in the Auger process is unaffected by the SMF, the ratio of complex DNA damage does not vary in the SMF.

Conclusion

This work investigated the dose distributions, electron ranges and the early DNA damage yields in magnetic fields by means of PHITS track-structure simulations. In macro scale evaluations, the projected range and the dose distribution for therapeutic high-energy electrons (MeV order) can be modulated by magnetic fields. However, in DNA-scale evaluations, early DNA damage yields in magnetic fields were found to be independent from the SMF intensity. These simulations suggest that the treatment planning for MRgRT can be made in consideration of both changes of dose distribution and unaffected by biological impact. Since the present simulation was performed only on physical processes, in the future it will be necessary to investigate chemical processes and the subsequent complex biological processes.

Declarations

Acknowledgement

This work was financially supported by the JAEA Fund for Exploratory Researches (Houga fund).

Conflict of Interest

The authors declare that they have no conflict of interest.

Author Contribution

Y. Yachi, T. Kai and Y. Matsuya designed the study. Y. Yachi, T. Kai and Y. Hirata performed Monte Carlo simulation for calculating the electron track structure in the static magnetic field. Y. Matsuya and Y. Yoshii supported the modelling of DNA damage induction. Y. Yachi wrote the manuscript. H. Date supervised the study. All authors reviewed the manuscript.

References

1. Lagendijk, JJ. et al. MRI/linac integration. *Radiother Oncol.* **86**(1): 25–9 (2008).
2. Mutic, S., Dempsey, J.F. The ViewRay system: magnetic resonance-guided and controlled radiotherapy. *Semin. Radiat. Oncol.* **24**(3):196–9 (2014).
3. Raaijmakers, A.J., Raaymakers, B.W., Lagendijk, J.J. Integrating a MRI scanner with a 6 MV radiotherapy accelerator: dose increase at tissue-air interfaces in a lateral magnetic field due to returning electrons. *Phys. Med. Biol.* **50**(7):1363–76 (2005).
4. Nakahara, T., Yaguchi, H., Yoshida, M. and Miyakoshi, J. Effects of exposure of CHO-K1 cells to a 10-T static magnetic field. *Radiology.* **224**(3): 817–22 (2002).
5. Takatsuji, T. Sasaki, M. S. and Takekoshi, H. Effect of static magnetic field on the induction of chromosome aberrations by 4.9 MeV protons and 23 MeV alpha particles. *J. Radiat. Res.* **30**(3): 238–246 (1989).
6. Inaniwa, T. et al. Effect of external magnetic fields on biological effectiveness of proton beams. *Int. J. Radiat. Oncol. Biol. Phys.* **106**(3): 597–603 (2020).
7. Inaniwa, T. et al. Enhancement of biological effectiveness of carbon-ion beams by applying a longitudinal magnetic field. *Int J Radiat Biol.* **95**(6): 720–724 (2019).
8. Rockwell, S. Influence of a 1400-gauss magnetic field on the radiosensitivity and recovery of EMT6 cells in vitro. *Int. J. Radiat. Biol.* **31**(2): 153–160 (1977).
9. Nath, R., Schulz, R. J. and Bongiorni, P. Response of mammalian cells irradiated with 30 MV X-rays in the presence of a uniform 20-kilogauss magnetic field. *Int. J. Radiat. Biol.* **38**(3): 285–292 (1980).
10. Wang, L. Biological responses of human solid tumor cells to X-ray irradiation within a 1.5-Tesla magnetic field generated by a magnetic resonance imaging-linear accelerator. *Bioelectromagnietics* **37**(7): 471–480 (2016).
11. Nikjoo, H. and Girard, P. A model of the cell nucleus for DNA damage calculations. *Int J Radiat Biol.* **88**(1-2): 87–97 (2012).
12. Friedland, W., Dingfelder, M., Kundrát, P. and Jacob, P. Track structures, DNA targets and radiation effects in the biophysical Monte Carlo simulation code PARTRAC. *Mutat Res.* **711**(1-2): 28–40 (2011).
13. Date, H., Sutherland, K. L., Hasegawa, H. and Shimozua, M. Ionization and excitation collision processes of electrons in liquid water. *Nucl. Instrum. Methods Phys. Res. B* **265**, 515–520 (2007).

14. Salvat, F. PENELOPE-2018: A Code System for Monte Carlo Simulation of Electron and Photon Transport. NEA/MBDAV/R(2019)1. ISBN: 9789264489950 (2019).
15. Sempau, J., Acosta, E., Baro, J., Fernández-Varea, J. M. and Salvat, F. An algorithm for Monte Carlo simulation of coupled electron-photon transport. *Nucl. Instrum. Methods Phys. Res. B* **132**(3): 377–390 (1997).
16. Incerti, S. et al. Geant4-DNA example applications for track structure simulations in liquid water: A report from the Geant4-DNA Project. *Med Phys.* **45**: e722-e739 (2018).
17. Bernal, M. A. et al. Track structure modeling in liquid water: A review of the Geant4-DNA very low energy extension of the Geant4 Monte Carlo simulation toolkit. *Phys Med.* **31**(8): 861–874 (2015).
18. Incerti, S. et al. Comparison of GEANT4 very low energy cross section models with experimental data in water. *Med Phys.* **37**(9): 4692–708 (2010).
19. Incerti, S. et al. The Geant4-DNA project. *Int. J. Model. Simul. Sci. Comput.* **1**(2): 157–178 (2010).
20. Kirkby, C., Stanescu, T. and Fallone, B. G. Magnetic field effects on the energy deposition spectra of MV photon radiation. *Phys. Med. Biol.* **54**: 243–257 (2009).
21. Bug, M. U. et al. Effect of a magnetic field on the track structure of low-energy electrons: a Monte Carlo study. *Eur. Phys. J. D* **60**: 85–92 (2010).
22. Sato, T. et al. Features of Particle and Heavy Ion Transport code System (PHITS) version 3.02. *J. Nucl. Sci. Technol.* **55**, 684–690 (2018).
23. Kai, T., Yokoya, A., Ukai, M., and Watanabe, R., Cross sections, stopping powers, and energy loss rates for rotational and phonon excitation processes in liquid water by electron impact. *Radiat. Phys. Chem.* **108**, 13–17 (2015).
24. Kai, T., Yokoya, A., Ukai, M., Fujii, K., and Watanabe, R. Dynamics of low energy electrons in liquid water with consideration of Coulomb interaction with positively charged water molecules induced by electron collision. *Radiat. Phys. Chem.* **102**, 16–22 (2014).
25. Kai, T., Yokoya, A., Ukai, M., and Watanabe, R. Deceleration processes of secondary electrons produced by a high-energy Auger electron in a biological context. *Int. J. Radiat. Biol.* **92**, 645–659 (2016).
26. Kai, T., Yokoya, A., Ukai, M., Fujii, K., and Watanabe, R. Thermal equilibrium and prehydration processes of electrons injected into liquid water calculated by dynamic Monte Carlo method. *Radiat. Phys. Chem.* **115**, 1–5 (2015).
27. Kai, T., Yokoya, A., Ukai, M., Fujii, K., and Watanabe, R. Dynamic behavior of secondary electrons in liquid water at the earliest stage upon irradiation: Implications for DNA damage localization mechanism. *J. Phys. Chem. A* **120**, 8228–8233 (2016).
28. Kai, T. et al. A significant role of non-thermal equilibrated electrons in the formation of deleterious complex DNA damage. *Phys. Chem. Chem. Phys.* **20**, 2838 (2018).
29. Matsuya, Y. et al. Modeling of yield estimation for DNA strand breaks based on Monte Carlo simulations of electron track structure in liquid water. *J. Appl. Phys.* **126**, 124701 (2019).

30. Matsuya, Y. et al. A simplified cluster analysis of electron track structure for estimating complex DNA damage yields. *Int. J. Mol. Sci.* **21**(5): 1701 (2020).
31. Matsuya, Y. et al. Track-structure mode in Particle and Heavy Ion Transport code System (PHITS): application to radiobiological research. *Int. J. Radiat. Biol.* (2021). DOI: 10.1080/09553002.2022.2013572.
32. Matsuya, Y.et al. Verification of KURBUC-based ion track structure mode for proton and carbon ions in the PHITS code. *Phys Med Biol.* **66**(6): 06NT02 (2021).
33. Hirayama, H., Namito, Y., Bielajew, A. F., Wilderman, S. J., and Nelson, W. R. The EGS5 code system. SLAC Report 730, prepared for the Department of Energy, USA (2005).
34. Nikjoo, H., O' Neill, P., Goodhead, D. T. and Terrissol, M. Computational modelling of low-energy electron-induced DNA damage by early physical and chemical events. *Int J Radiat Biol.* **71**(5): 467–83 (1997).

Figures

Figure 1

Dose distribution of electrons in SMFs. Dose distributions along the x-axis (A) and y-axis (B) for 10-MeV incident electrons in the positive y-axis direction parallel to the SMF (see (C)) calculated by EGS. The distributions along the x-axis (D) and z-axis (E) for 1-MeV incident electrons in the positive z-axis direction perpendicular to the SMF (see (F)) calculated by EGS. We confirmed that the distributions calculated by *etsmode* were in good agreement with those by EGS as shown in supplementary data (Fig. S2). The distributions for 10-MeV and 1-MeV electrons were significantly affected by the SMFs.

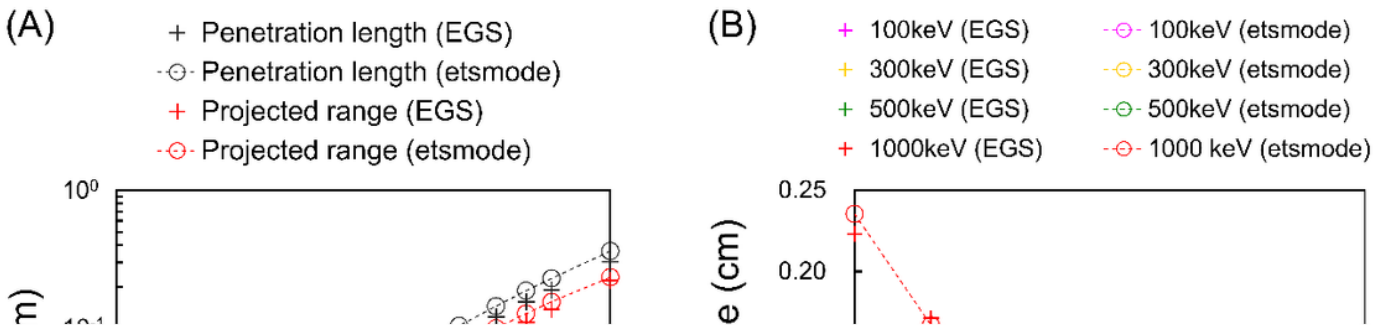

Figure 2

Electron ranges in SMFs calculated by *etsmode* and EGS. (A) shows the penetration length and projected range in the absence of a SMF (B = 0.0 T) and (B) shows the projected range in the presence of various SMF strengths (B = 0.0-10.0 T). The simulation results by *etsmode* and EGS are in good agreement with each other. As shown in Fig. 2 (B), the projected range of high-energy electrons is largely affected by the SMF strength.

Figure 3

Gyration time and radius of electron tracks in vacuum applied by magnetic fields. (A) shows the time and radius of monoenergetic electrons in vacuum calculated by DMCC. (B) shows the radius of monoenergetic electrons in vacuum (blue circles) calculated by DMCC. The radius in vacuum was compared to the projected range in B = 0.0 (T) (cross symbols) and that in B = 3.0 T (plus symbols).

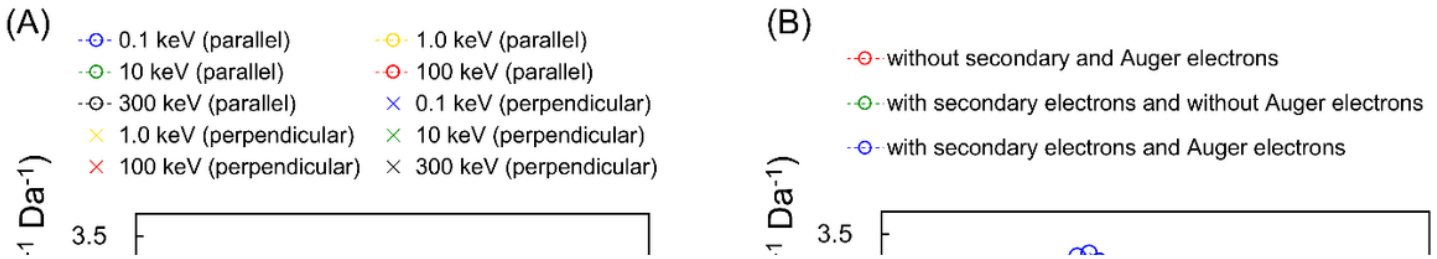

Figure 4

Yields of DSBs for monoenergetic electrons in SMFs. (A) shows the Y_{DSB} values for mono-energetic electrons with 0.1-300 keV electrons in the SMFs (B = 0.0-10.0 (T)). (B) shows the Y_{DSB} values without considering secondary electrons, including Auger electrons. The Y_{DSB} values were calculated using PHITS (v. 3.26) and an analytical code for estimating DNA damage yields.[29]

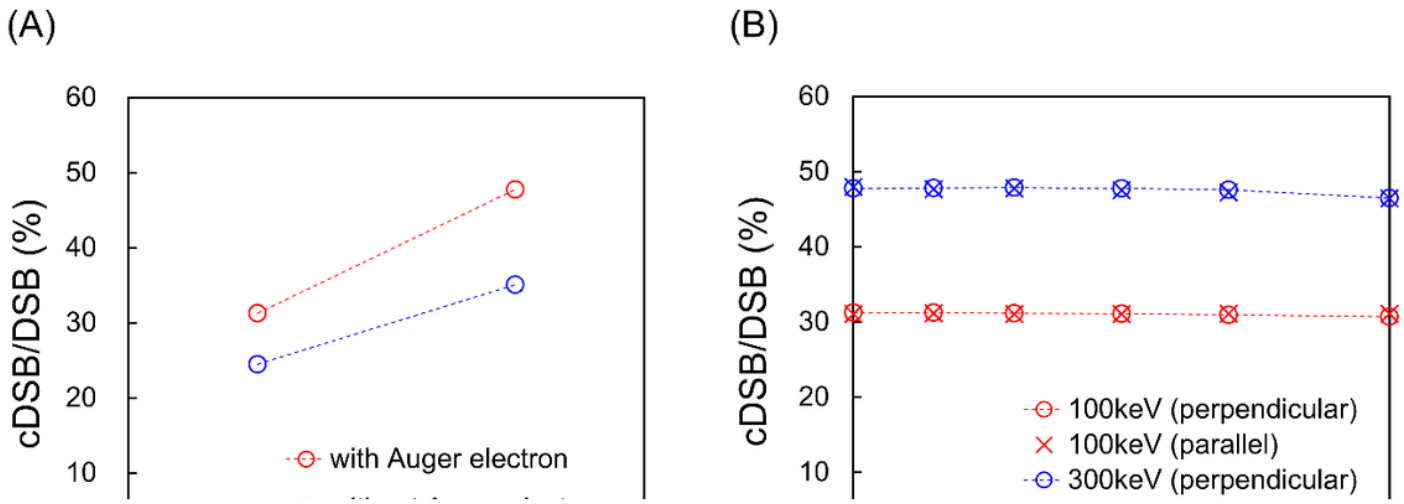

Figure 5

Various calculation results related complex DNA damage induction. (A) shows the relationship between the ratio of complex DSB yields per all DSBs yields (cDSB/DSB) and electron energy (100 and 300 keV). (B) shows the cDSB/DSB for 100 keV, 300 keV electrons for various intensities of SMF, which is the ratio of the complex DSB yields calculated using PHITS (v. 3.26) and an analytical code for estimating DNA damage yields[30].

Supplementary Files

This is a list of supplementary files associated with this preprint. Click to download.

- SupplementaryDataYachi2022.01.11.docx